

## Absence of magnetic long range order in $\text{Ba}_3\text{ZnRu}_2\text{O}_9$ : A spin-liquid candidate in the $S = 3/2$ dimer lattice

Ichiro Terasaki<sup>1\*</sup>, Taichi Igarashi<sup>1</sup>, Takayuki Nagai<sup>1</sup>, Kenji Tanabe<sup>1</sup>, Hiroki Taniguchi<sup>1</sup>, Taku Matsushita<sup>1</sup>, Nobuo Wada<sup>1</sup>, Atsushi Takata<sup>2</sup>, Takanori Kida<sup>2</sup>, Masayuki Hagiwara<sup>2</sup>, Kensuke Kobayashi<sup>3</sup>, Hajime Sagayama<sup>3</sup>, Reiji Kumai<sup>3</sup>, Hironori Nakao<sup>3</sup>, and Youichi Murakami<sup>3</sup>

<sup>1</sup>*Department of Physics, Nagoya University, Nagoya 464-8602, Japan*

<sup>2</sup>*Center for Advanced High Magnetic Field Science, Graduate School of Science, Osaka University, 1-1 Machikaneyama, Toyonaka, Osaka 560-0043, Japan*

<sup>3</sup>*Condensed Matter Research Center and Photon Factory, Institute of Materials Structure Science, High Energy Accelerator Research Organization, Tsukuba 305-0801, Japan*

We have discovered a novel candidate for a spin liquid state in a ruthenium oxide composed of dimers of  $S = 3/2$  spins of  $\text{Ru}^{5+}$ ,  $\text{Ba}_3\text{ZnRu}_2\text{O}_9$ . This compound lacks a long range order down to 37 mK, which is a temperature 5000-times lower than the magnetic interaction scale of around 200 K. Partial substitution for Zn can continuously vary the magnetic ground state from an antiferromagnetic order to a spin-gapped state through the liquid state. This indicates that the spin-liquid state emerges from a delicate balance of inter- and intra-dimer interactions, and the spin state of the dimer plays a vital role. This unique feature should realize a new type of quantum magnetism.

Since Anderson proposed the idea of a quantum spin liquid as a possible ground state for a spin-half ( $S = 1/2$ ) antiferromagnetic triangular lattice<sup>1)</sup> with a suppressed long-range magnetic ordering due to geometrical frustration and quantum fluctuations of interacting spins, researchers have sought this state of quantum matter.<sup>2)</sup> A quantum spin liquid should possess a ground state consisting of highly entangled singlet-spin pairs and exotic excited states called spinons.<sup>3,4)</sup> Although several candidates have been reported experimentally, none has been confirmed. Organic candidates consist of ill-defined localized magnetic moments where the magnetic exchange interaction is comparable to the charge gap.<sup>5-7)</sup> On the other hand, inorganic candidates suffer from unwanted disorder/impurity/nonstoichiometry.  $\text{Na}_4\text{Ir}_3\text{O}_8$ <sup>8)</sup> shows a spin-glass-like transition near 6–7 K,<sup>9,10)</sup> whereas  $\text{ZnCu}_3(\text{OH})_6\text{Cl}_2$ <sup>11)</sup> and  $\text{Ba}_3\text{CuSb}_2\text{O}_9$ <sup>12)</sup> include a considerable intermixture of cations.  $\text{BaCu}_3\text{V}_2\text{O}_8(\text{OH})_2$ <sup>13)</sup> and 6H-B  $\text{Ba}_3\text{NiSb}_2\text{O}_9$ <sup>14)</sup> have a substantial low-temperature Curie tail due to unwanted impurities. In the case of  $\text{BaCu}_3\text{V}_2\text{O}_8(\text{OH})_2$ , an inhomogeneous magnetic order has been detected through NMR measurements around 9 K, below which the unwanted Curie tail grows rapidly.<sup>15,16)</sup>

We have discovered the absence of magnetic long range order in a hexagonal lattice of  $\text{Ru}^{5+}$  dimers in  $\text{Ba}_3\text{ZnRu}_2\text{O}_9$  down to 37 mK, where neither Curie tail nor glassy behavior is detected. The magnetic specific heat shows no anomaly below 80 K, and is found to be linear in temperature below around 5 K. These thermodynamic measurements suggest a spin-liquid like ground state in this oxide. The  $\text{Ru}^{5+}$  ion acts as a well-localized  $S = 3/2$  spin, and the spin liquid is totally unprecedented in such a large spin.

Polycrystalline samples of  $\text{Ba}_3\text{MRu}_2\text{O}_9$  ( $M = \text{Zn}, \text{Co}$  and  $\text{Co}$ ) were prepared with solid state reaction. Stoichiometric mixtures of powdered oxide or carbonate sources ( $\text{BaCO}_3$ ,  $\text{RuO}_2$ ,  $\text{Co}_3\text{O}_4$ ,  $\text{ZnO}$ ,  $\text{CaCO}_3$ ) were ground in an agate mortar, and were pre-sintered in air at 1273 K for 12 h. The pre-

sintered powders were finely ground, pressed into pellets, and sintered in air at 1473 K for 72 h.

The synchrotron x-ray diffraction was taken at BL8A&8B, Photon-Factory, KEK, Japan. The energy of the x-ray was adjusted to be 18 keV, which was carefully calibrated using a standard powder sample of  $\text{CeO}_2$ . Powder samples were sealed in a silica-glass capillary of 0.1-mm diameter, and the capillary was rotated by an angle of 30 deg from the sample-stage axis during measurement. The diffraction patterns were analyzed using the Rietveld refinement with Rietan-FP code.<sup>17)</sup> The magnetic susceptibility was measured with a commercial susceptometer (Quantum Design MPMS) above 2 K, and with a home-made probe equipped with a SQUID sensor in a dilution refrigerator down to 37 mK in various external fields up to 7 mT. The signal of the sensor was calibrated with the measured data using MPMS from 2 to 4 K. The magnetization at 1.4 K up to 50 T was measured in pulsed fields by an induction method at Center for Advanced High Magnetic Field Science in Osaka University. The specific heat was measured with a commercial measurement system (Quantum Design PPMS). The ac resistivity was measured with an LCR meter (Agilent E4980A) with a frequency of 10 kHz.

Figure 1(a) schematically shows the crystal structure of  $\text{Ba}_3\text{MRu}_2\text{O}_9$ .<sup>18)</sup> The two face-shared  $\text{RuO}_6$  octahedra ( $\text{Ru}_2\text{O}_9$  dimer block) form a layered structure, and are interconnected through the  $\text{MO}_6$  octahedron along the  $c$ -axis in a corner-shared arrangement. The  $\text{Ru}^{5+}$  ion with an electronic configuration of  $(4d)^3$  acts as a local moment of  $S = 3/2$  and is responsible for the magnetism of  $\text{Ba}_3\text{MRu}_2\text{O}_9$ .

Figure 1(b) depicts the in-layer arrangement of the  $\text{Ru}_2\text{O}_9$  dimer blocks, where each block is connected with three neighboring  $\text{MO}_6$  octahedra to form a hexagonal dimer lattice. The species of  $M$  determines the magnetic ground state. For  $M = \text{Co}, \text{Ni}$ , and  $\text{Cu}$ , the system exhibits an antiferromagnetic order below around  $T_N = 100$  K.<sup>18-20)</sup> The nearly identical  $T_N$  for the different species of  $M$  implies that the magnetic mo-

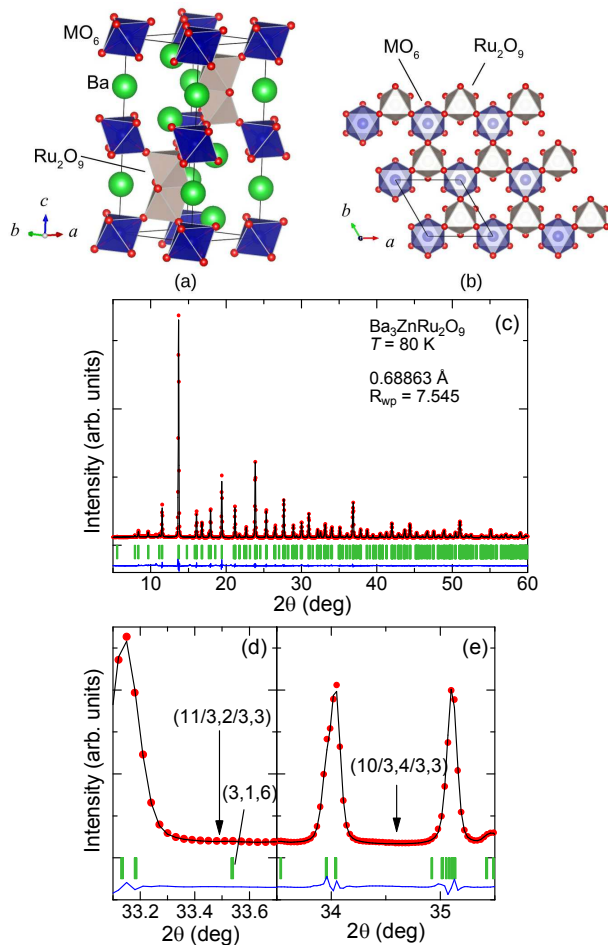


**Fig. 1.** Crystal structure of  $\text{Ba}_3\text{MRu}_2\text{O}_9$ . (a) Layered structure where the two face-shared  $\text{RuO}_6$  octahedra (the  $\text{Ru}_2\text{O}_9$  dimer) and the  $\text{MO}_6$  octahedron are alternately stacked along the  $c$ -axis. (b) The  $ab$  plane layer where the  $\text{Ru}_2\text{O}_9$  dimer and  $\text{MO}_6$  form an edge-shared network to construct a hexagonal dimer lattice of  $\text{Ru}^{5+}$ . (c) The synchrotron x-ray diffraction pattern and the Rietveld refinement of  $\text{Ba}_3\text{ZnRu}_2\text{O}_9$  at 80 K. (d)(e) The magnified view of the diffraction pattern. The arrow indicates a position of possible superlattice reflection to probe inter-cation mixture of Zn and Ru.

ment of the  $M$  ions plays a secondary role. For  $M = \text{Ca}$  and  $\text{Sr}$ , the ground state is a nonmagnetic spin-gapped state, in which the two localized spins in the  $\text{Ru}_2\text{O}_9$  dimer block form a singlet pair.<sup>19,21,22)</sup>

Figure 1(c) shows the synchrotron x-ray diffraction pattern and the Rietveld refinement of  $\text{Ba}_3\text{ZnRu}_2\text{O}_9$  at 80 K. As shown in the figure, the refinement is satisfactory, and we have verified the crystal structure shown in Figs. 1(a) and 1(b) (Space group  $\text{P}63/\text{mmc}$  (No.194),  $a = 5.7576 \text{ \AA}$ ,  $c = 14.1424 \text{ \AA}$ ). We also emphasize that no trace of impurity phases is detected, and the sample is pure enough to discuss the thermodynamic properties of the main phase. Figures 1(d) and 1(e) show the magnified view of the diffraction pattern. The arrow indicates a position of possible superlattice reflections, if an inter-mixture of Zn and Ru happened as in the case of  $\text{Ba}_3\text{CuSb}_2\text{O}_9$ .<sup>12)</sup> No trace of such reflection peaks safely excludes the possibility of the Zn-Ru inter-mixture.

Figure 2(a) plots the magnetic susceptibility of  $\text{Ba}_3\text{MRu}_2\text{O}_9$  for  $M = \text{Co}$ ,  $\text{Zn}$ , and  $\text{Zn}_{0.3}\text{Ca}_{0.7}$  on a logarithmic scale. Although an antiferromagnetic transition occurs for the  $M = \text{Co}$  sample as a kink around 100 K, a much smaller

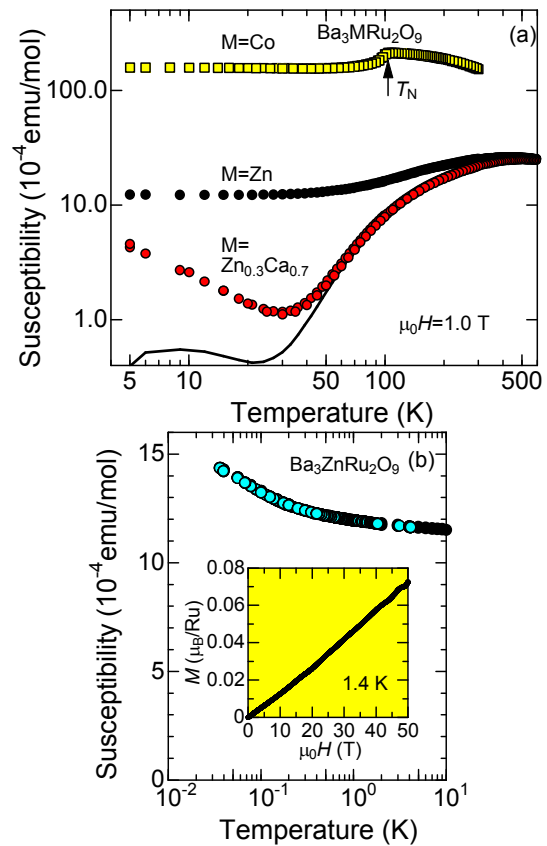


**Fig. 2.** (a) Magnetic susceptibility of  $\text{Ba}_3\text{MRu}_2\text{O}_9$  above 4 K. Upturn toward low temperatures for  $M = \text{Zn}_{0.3}\text{Ca}_{0.7}$  is due to the 0.1% contribution of unwanted magnetic impurities. Solid curve denotes the intrinsic susceptibility of  $M = \text{Zn}_{0.3}\text{Ca}_{0.7}$  obtained by subtracting of the low-temperature Curie term. (b) Magnetic susceptibility below 10 K for  $\text{Ba}_3\text{ZnRu}_2\text{O}_9$ . No sign of a phase transition is detected down to 37 mK. The inset shows the magnetization  $M$  plotted as a function of external field  $\mu_0 H$  at 1.4 K.

susceptibility is observed for the  $M = \text{Zn}_{0.3}\text{Ca}_{0.7}$  sample. If the low-temperature Curie tail is subtracted by assuming a tiny contribution (0.1 mol %) of an unwanted magnetic impurity, the solid curve shows the intrinsic susceptibility. The curve gives a nearly temperature-independent value of  $10^{-5} \text{ emu/mol}$  below 20 K, which can be assigned to the Van Vleck susceptibility of the Ru ions.

The  $M = \text{Zn}$  sample shows a magnetic susceptibility intermediate between the  $M = \text{Co}$  and  $\text{Zn}_{0.3}\text{Ca}_{0.7}$  samples, which is roughly consistent with a very recent report.<sup>23)</sup> This sample shows a weakly temperature-dependent susceptibility with a broad maximum around 400 K without any trace of a cusp or discontinuity down to 37 mK (Fig. 2(b)). A Curie tail is not visible throughout the measured temperature ranges, whereas the susceptibility weakly increases with decreasing temperature below 1 K. The inset of Fig. 2(b) shows the magnetization plotted as a function of external field up to 50 T at 1.4 K. The linear and reversible behaviour indicates an antiferromagnetic interaction larger than 50 T. If magnetic impurities were present, the magnetization curve should be convex upward as can be explained with the Brillouin function. If the system were in a glassy state as seen in  $\text{BaCu}_3\text{V}_2\text{O}_8(\text{OH})_2$ ,<sup>13)</sup> the magnetization should saturate at high fields. The present magnetization curve excludes a possible existence of free magnetic impurities and/or glassy states. Previous neutron diffrac-

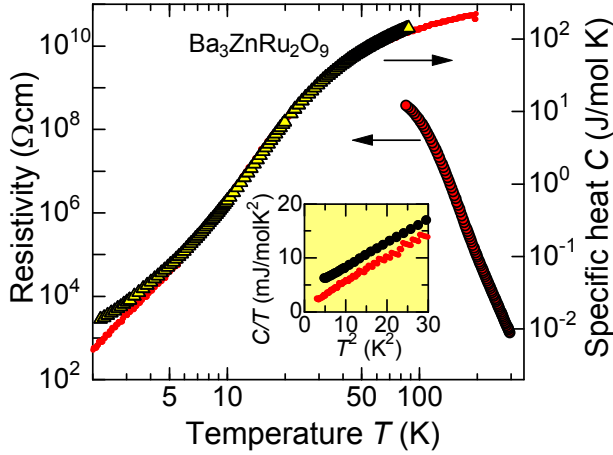


**Fig. 3.** Resistivity and specific heat of  $\text{Ba}_3\text{ZnRu}_2\text{O}_9$  plotted as a function of temperature  $T$ . Inset plots  $C/T$  as a function of  $T^2$  where the gapless  $T$ -linear contribution of  $C$  is evaluated to be  $4 \text{ mJ/mol K}^2$ . The small dotted data represent the specific heat of a non-magnetic reference material  $\text{Ba}_3\text{ZnSb}_2\text{O}_9$  taken from Ref.<sup>14)</sup>

tion studies have also reported no long range order.<sup>18,23)</sup> Therefore, these results strongly indicate that this paramagnetism is due to a quantum spin-liquid state.

Let us evaluate the magnitude of the intra-dimer exchange energy. Darret et al.<sup>21)</sup> first analyzed the susceptibility of  $\text{Ba}_3\text{MR}_2\text{O}_9$  ( $M = \text{Ca}, \text{Mg}, \text{Cd}$ ) assuming independent spin dimers, and evaluated the intra-dimer interaction  $J_{\text{intra}}$  to be around 200 K. Later Senn et al. evaluated  $J_{\text{intra}}$  to be 240 K for  $\text{Ba}_3\text{CaRu}_2\text{O}_9$ .<sup>22)</sup> In an LDA+U calculation for  $\text{Ba}_3\text{CoZn}_2\text{O}_9$ , Streltsov<sup>24)</sup> theoretically evaluated  $J_{\text{intra}}$  to be 150 K. Thus we can conclude that magnetic phase transition is not detected at temperatures 5000 times lower than the interaction energy scale in  $\text{Ba}_3\text{ZnRu}_2\text{O}_9$ .

Figure 3 shows the resistivity and specific heat of  $\text{Ba}_3\text{ZnRu}_2\text{O}_9$ . The resistivity is as high as  $10^3 \text{ } \Omega\text{cm}$  at room temperature, and increases up to  $10^8 \text{ } \Omega\text{cm}$  at 100 K. This highly insulating behavior eliminates the possibility that the susceptibility of this oxide is due to simple Pauli paramagnetism. The temperature dependence near 300 K implies that the activation energy is around 2000 K, which greatly exceeds  $J_{\text{intra}} = 150\text{--}240 \text{ K}$ . These observations indicate that the electrons are well localized in this oxide, justifying that localized magnetic moments are responsible for the magnetism.

The specific heat does not show an anomaly from 80 down to 2 K, indicating the absence of a thermodynamic phase transition. The inset shows the existence of a temperature-linear contribution in the specific heat, which is evaluated to be  $4 \text{ mJ/mol K}^2$  for  $T \rightarrow 0$ . The specific heat does not exhibit a Schottky anomaly above 2 K, which is consistent with the absence of a Curie tail in the susceptibility. The linear dependence is most likely from spinons and not simple magnons. The magnitude is on the same order as the electron specific heat coefficient of alkaline metals, providing evidence of gapless excitations in the spin sector. In order to examine the magnetic contribution, we plot the specific heat of  $\text{Ba}_3\text{ZnSb}_2\text{O}_9$  taken from Ref.<sup>14)</sup> as a non-magnetic reference material. As is clearly seen, the specific heat of the two samples is almost identical above 10 K, and the magnetic contribution of Ru is hidden in the overwhelming major contribu-

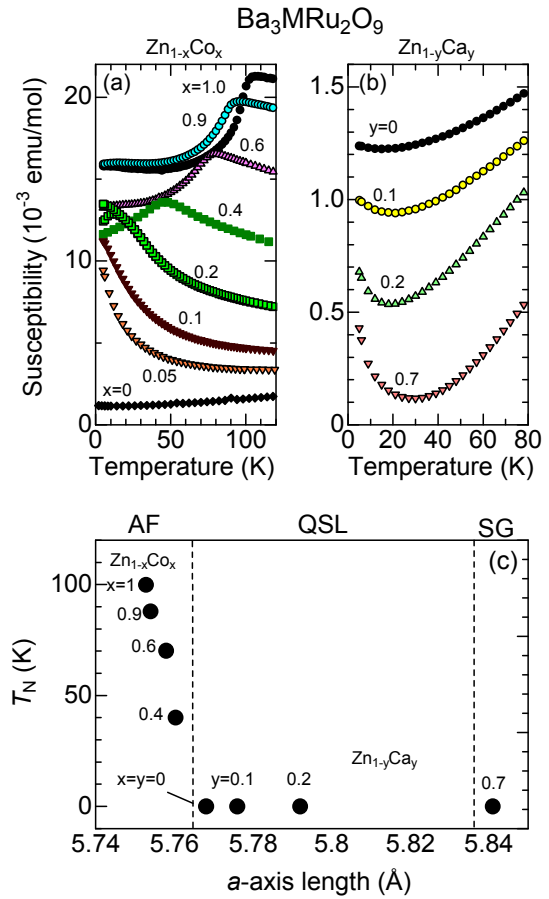


**Fig. 4.** Magnetic susceptibility of (a)  $\text{Ba}_3\text{Zn}_{1-x}\text{Co}_x\text{Ru}_2\text{O}_9$  and (b)  $\text{Ba}_3\text{Zn}_{1-y}\text{Ca}_y\text{Ru}_2\text{O}_9$ . (c) Transition temperature plotted as a function of the  $a$ -axis length (the inter-dimer distance). Dotted lines indicate the approximate phase boundaries determined from (a) and (b). AF, QSL, and SG stand for antiferromagnetically ordered state, quantum spin-liquid state and spin-gapped state, respectively.

tion from the lattice. The inset shows that the specific heat of  $\text{Ba}_3\text{ZnSb}_2\text{O}_9$  has the identical  $T^3$  term without  $T$ -linear term. This indicates that the magnetic contribution is proportional to  $T$  in  $\text{Ba}_3\text{ZnRu}_2\text{O}_9$  at low temperatures.

A unique feature of  $\text{Ba}_3\text{MRu}_2\text{O}_9$  is that the magnetic ground state can be finely tuned from the antiferromagnetic order to the non-magnetic spin-gapped state through the gapless quantum spin-liquid state. Figures 4(a) and (b) show the magnetic susceptibility of  $\text{Ba}_3\text{Zn}_{1-x}\text{Co}_x\text{Ru}_2\text{O}_9$  and  $\text{Ba}_3\text{Zn}_{1-y}\text{Ca}_y\text{Ru}_2\text{O}_9$ , respectively. The susceptibility at 120 K systematically increases with the Co concentration  $x$ , because the magnetic  $\text{Co}^{2+}$  ion contributes to the susceptibility in  $\text{Ba}_3\text{Zn}_{1-x}\text{Co}_x\text{Ru}_2\text{O}_9$ . Simultaneously, the antiferromagnetic transition temperature systematically increases with  $x$ . The 20% Co substituted sample ( $x = 0.2$ ) shows a temperature hysteresis below approximately 15 K, which can be assigned to a glass transition. For  $x < 0.2$ , the system seems to be in a spin-liquid state. For Ca substitution, the  $y = 0.2$  sample shows a finite paramagnetic contribution around 20 K and is still in the spin-liquid state. The magnitude continuously decreases with  $y$ , implying a magnetically inhomogeneous state such as a mixture of spin-liquid and spin-gapped states.

Here we discuss a possible microscopic mechanism to cause various magnetic ground states in  $\text{Ba}_3\text{MRu}_2\text{O}_9$ . Figure

4 (c) plots the transition temperature as a function of the  $a$ -axis length, or equivalently, the inter-dimer distance. The two dotted lines represent the phase boundary determined from Figs. 4(a) and 4(b). First of all, we emphasize that the inter-dimer interaction competes with the intra-dimer interaction ( $J_{\text{intra}}=150\text{--}240$  K) in this family, if the number of the nearest neighbor dimers ( $z = 6$ ) is taken into account. According to the LDA+U calculation,<sup>24)</sup> the interaction  $J_{\text{inter}}$  along the Ru–O–O–Ru network between the neighboring dimers is evaluated to be 30–40 K, and we arrive at the particular condition  $zJ_{\text{inter}} \sim J_{\text{intra}}$ . We further note that the interaction between Co and Ru is evaluated to be less than 8 K, being much smaller than  $J_{\text{inter}}$ . Thus, even though the magnetism of  $\text{Co}^{2+}$  ions complicates the magnetic structure, we may safely ignore this in the lowest approximation. We expect that the  $a$ -axis length changes  $J_{\text{inter}}$ ; For a short  $a$ , the condition  $zJ_{\text{inter}} > J_{\text{intra}}$  stabilizes the antiferromagnetic order, whereas for a long  $a$ ,  $zJ_{\text{inter}} < J_{\text{intra}}$  favors the spin singlet within dimers. We expect that the quantum spin-liquid state can emerge from a delicate condition of  $zJ_{\text{inter}} \sim J_{\text{intra}}$ .

In summary, we have discovered that no magnetic transitions occur down to 37 mK in  $\text{Ba}_3\text{ZnRu}_2\text{O}_9$ . The  $T$ -linear magnetic specific heat and the paramagnetic susceptibility strongly suggest a quantum spin liquid state. Considering that the related oxides show the antiferromagnetic order or the spin-gapped nonmagnetic state, we suggest that competing interaction between intra- and inter-dimer interactions should stabilize this spin liquid like state.

The authors would like to thank Chisa Hotta and Yukio Yasui for fruitful discussion and useful advice. This work was partially supported by Grant-in-Aid for Scientific Research and a Grant-in-Aid for JSPS Fellows, Japan Society for the Promotion of Science, Japan (Kakenhi Nos. 25610091, 26247060, 15J04615), and by Program for Leading Graduate Schools “Integrative Graduate Education and Research in Green Natural Sciences”, MEXT, Japan. The synchrotron x-ray diffraction was performed under the approval of the Photon Factory Program Advisory Committee (Proposal Nos. 2012G718 and 2012S2-005).

- M. A. Green, and C. Broholm: *Science* **336** (2012) 559.
- 13) Y. Okamoto, H. Yoshida, and Z. Hiroi: *J. Phys. Soc. Jpn.* **78** (2009) 033701.
  - 14) J. G. Cheng, G. Li, L. Balicas, J. S. Zhou, J. B. Goodenough, C. Xu, and H. D. Zhou: *Phys. Rev. Lett.* **107** (2011) 197204.
  - 15) J. A. Quilliam, F. Bert, R. H. Colman, D. Boldrin, A. S. Wills, and P. Mendels: *Phys. Rev. B* **84** (2011) 180401.
  - 16) M. Yoshida, Y. Okamoto, M. Takigawa, and Z. Hiroi: *J. Phys. Soc. Jpn.* **82** (2013) 013702.
  - 17) F. Izumi and F. Momma: *Solid State Phenom.* **130** (2007) 15.
  - 18) P. Lightfoot and P. Battle: *J. Solid State Chem.* **89** (1990) 174.
  - 19) I. Fernandez, R. Greatrex, and N. N. Greenwood: *J. Solid State Chem.* **34** (1980) 121.
  - 20) J. Rijssenbeek, Q. Huang, R. Erwin, H. Zandbergen, and R. Cava: *J. Solid State Chem.* **146** (1999) 65.
  - 21) J. Darriet, M. Drillon, G. Villeneuve, and P. Hagenmuller: *J. Solid State Chem.* **19** (1976) 213.
  - 22) M. S. Senn, A. M. Arevalo-Lopez, T. Saito, Y. Shimakawa, and J. P. Attfield: *J. Phys.: Condens. Mat.* **25** (2013) 496008.
  - 23) P. Beran, S. Ivanov, P. Nordblad, S. Middey, A. Nag, D. Sarma, S. Ray, and R. Mathieu: *Solid State Sci.* **50** (2015) 58.
  - 24) S. V. Streltsov: *Phys. Rev. B* **88** (2013) 024429.

1) P. Anderson: *Mater. Res. Bull.* **8** (1973) 153.

2) L. Balents: *Nature* **464** (2010) 199.

3) S.-S. Lee and P. A. Lee: *Phys. Rev. Lett.* **95** (2005) 036403.

4) P. A. Lee, N. Nagaosa, and X.-G. Wen: *Rev. Mod. Phys.* **78** (2006) 17.

5) Y. Shimizu, K. Miyagawa, K. Kanoda, M. Maesato, and G. Saito: *Phys. Rev. Lett.* **91** (2003) 107001.

6) T. Itou, A. Oyamada, S. Maegawa, M. Tamura, and R. Kato: *Phys. Rev. B* **77** (2008) 104413.

7) T. Isono, H. Kamo, A. Ueda, K. Takahashi, M. Kimata, H. Tajima, S. Tsuchiya, T. Terashima, S. Uji, and H. Mori: *Phys. Rev. Lett.* **112** (2014) 177201.

8) Y. Okamoto, M. Nohara, H. Aruga-Katori, and H. Takagi: *Phys. Rev. Lett.* **99** (2007) 137207.

9) R. Dally, T. Hogan, A. Amato, H. Luetkens, C. Baines, J. Rodriguez-Rivera, M. J. Graf, and S. D. Wilson: *Phys. Rev. Lett.* **113** (2014) 247601.

10) A. C. Shockley, F. Bert, J.-C. Orain, Y. Okamoto, and P. Mendels: *Phys. Rev. Lett.* **115** (2015) 047201.

11) M. P. Shores, E. A. Nytko, B. M. Bartlett, and D. G. Nocera: *J. Am. Chem. Soc.* **127** (2005) 13462.

12) S. Nakatsuji, K. Kuga, K. Kimura, R. Satake, N. Katayama, E. Nishibori, H. Sawa, R. Ishii, M. Hagiwara, F. Bridges, T. U. Ito, W. Hig-